New Journal of Physics

Formation of spiral structures and radial convection in the edge region of a magnetized rotating plasma

R Barni[1], C Riccardi[1,3], Th Pierre[2], G Leclert[2], A Escarguel[2], D Guyomarc'h[2] and K Quotb[2]

[1] Dipartimento di Fisica Occhialini, Università degli Studi di Milano-Bicocca, p.za della Scienza 3, 20126 Milano, Italy
[2] Laboratoire PIIM, UMR 6633, CNRS et Université de Provence, 13397 Marseille Cedex 20, France
E-mail: claudia.riccardi@mib.infn.it

Abstract. The rotation of a cylindrical plasma column in a magnetic field has been studied in the linear section of the new plasma device Mistral. Under suitable conditions we observe a transition to a turbulent regime characterized by strong, bursty fluctuations at the edge of the column. The detection and the study of the spatio-temporal evolution of structures in the turbulent regime have been performed by means of a new enhanced conditional sampling technique. We have collected evidence of the development of a bent tail emanating from the plasma column. The charged particles inside the structure move along a spiral trajectory resulting in a net radial convection of the plasma to the walls. We show experimentally that a poloidal electric field is present inside the structures leading to the observed outwards radial $\mathbf{E} \times \mathbf{B}$ drift, in agreement with the expectations of recent and past theoretical works.

[3] Author to whom any correspondence should be addressed.

Contents

1. Introduction

The statistical properties of plasma turbulence in magnetically confined plasmas have been studied for many years in an attempt to understand their effect on anomalous transport and to gain insight into the underlying basic processes. So far turbulence-induced transport is indeed a major stumbling block affecting the performances of fusion-aimed devices. In recent years, the intermittent nature of this phenomenon has been revisited [1], focusing towards the role of burst-like fluctuations in the transport both in tokamak scrape-off layers (SOLs) [2–4] and in other magnetized plasmas, including stellarators [5, 6], reversed field pinches [13], simple magnetized tori (SMT) [7–10] and linear Q-machines [11, 12]. This kind of structure, indicated in the literature sometimes as intermittent plasma objects (IPOs) [2], avalanches or avaloids [4, 12] and even as coherent vortical structures [7, 13, 14], displays a convective dynamics and many similarities, which prompted the claim of some sort of universality [4]. Moreover such long-lived structures are advected in the background plasma to the walls contributing to a large extent both to particle and to energy transport [2, 15, 16]. While in curved devices the electric polarization induced by the curvature of the magnetic field lines is an obvious source for the convective motion, in a linear magnetized plasma column other mechanisms should come into play in order to drive a radial convection of the structures. In the relevant literature concerning linear devices, the onset of turbulence is generally ascribed to the diamagnetic drift wave instability [17, 18] or to the Kelvin–Helmholtz shear flow instability [11]. However, in the case of a longitudinally magnetized plasma column, the equilibrium radial electric field induces a poloidal $\mathbf{E} \times \mathbf{B}$ rotation of the column and a 'gravitational' drift happens due to the centrifugal effects in the rotating plasmas. While numerous studies were devoted to the centrifugal instability in the decade 1970–1980 [19–21], this effect was subsequently mainly ignored in the literature and only recently the possible role of the centrifugal force in the anomalous transport was pointed out again [22, 23]. Quite interestingly, centrifugal effects have been proposed recently also in fusion research as a different confinement scheme [24]. Besides the origin of the instability leading to anomalous transport phenomena, the role of the $\mathbf{E} \times \mathbf{B}$ drift velocity in the non-linear cross-field advection of plasma structures is actively investigated [25, 26].

    In the Mistral plasma device, a steady magnetized plasma column can be produced. By controlling the operating parameters, the column can be put in rotation about its axis. Under suitable conditions the system undergoes a transition to a turbulent regime, which constitutes the aim of the present paper. The starting point was the observation of spiral plasma structures in the regular plasma state [27], which shows strong similarities with the form predicted by theory
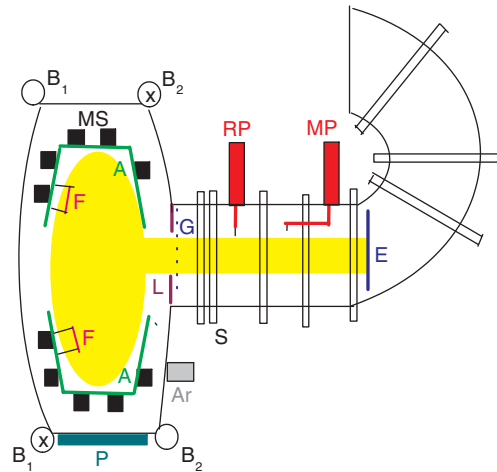
Figure 1. The schematic setup of the Mistral device. The measurements have been performed in the linear part of the device, where a rotating magnetized plasma column is produced and its turbulent regime is studied. MS, multipolar structure; F, filaments for cathode; A, anode; Ar, argon gas inlet; P, pumping; B1 and B2, compensation coils; S, solenoid; L, limiter; G, biased grid; E, end plate; MP, movable Langmuir probe; RP, reference probe.

under the action of the centrifugal force [28]. Radial convection of plasma structures has been observed in the turbulent regime too [29]. The spatio-temporal evolution shows the development of an elongated tail expanding radially outwards and bent into a spiral, possibly due to the differential rotation velocity. Here we present the detailed results of the experimental study of the structures and their motion in the turbulent state of the device. The paper is organized as follows: after a brief description of the device and the experimental setup, we discuss the diagnostic system and the analysis tools employed. Then we present the experimental results concerning the spatio-temporal evolution of the structures in the turbulent regime.

2. The experimental setup

The Mistral device was developed at the Laboratoire PIIM in Marseille in order to study the turbulence and transport in magnetized plasmas. Research spans from dynamical control to direct imaging of turbulence [30]. The device has been well characterized already and it is described in detail in a recent paper [27]. We discuss here only the features which have a direct influence on the issues concerning our aims.

The setup is sketched in figure 1. The plasma is produced by a large multipolar source, operating a low pressure ($P = 1$–5×10^{-2} Pa) discharge in argon within the main chamber. A steady discharge is sustained by the thermoelectronic emission of 32 hot tungsten filaments, which act as cathode. The total current I_f flowing in the filaments is one of the operating parameters of the device, while the potential difference between the cathode and the anode V_b is another. The surrounding grid plate constitutes the anode, which can be held at a fixed potential V_a with respect to the grounded vacuum chamber walls. A floating grid, which can be biased, separates the source from the linear (diameter $D = 40$ cm) and the semicircular part of the solenoid ($B_{\max} = 0.03$ T).
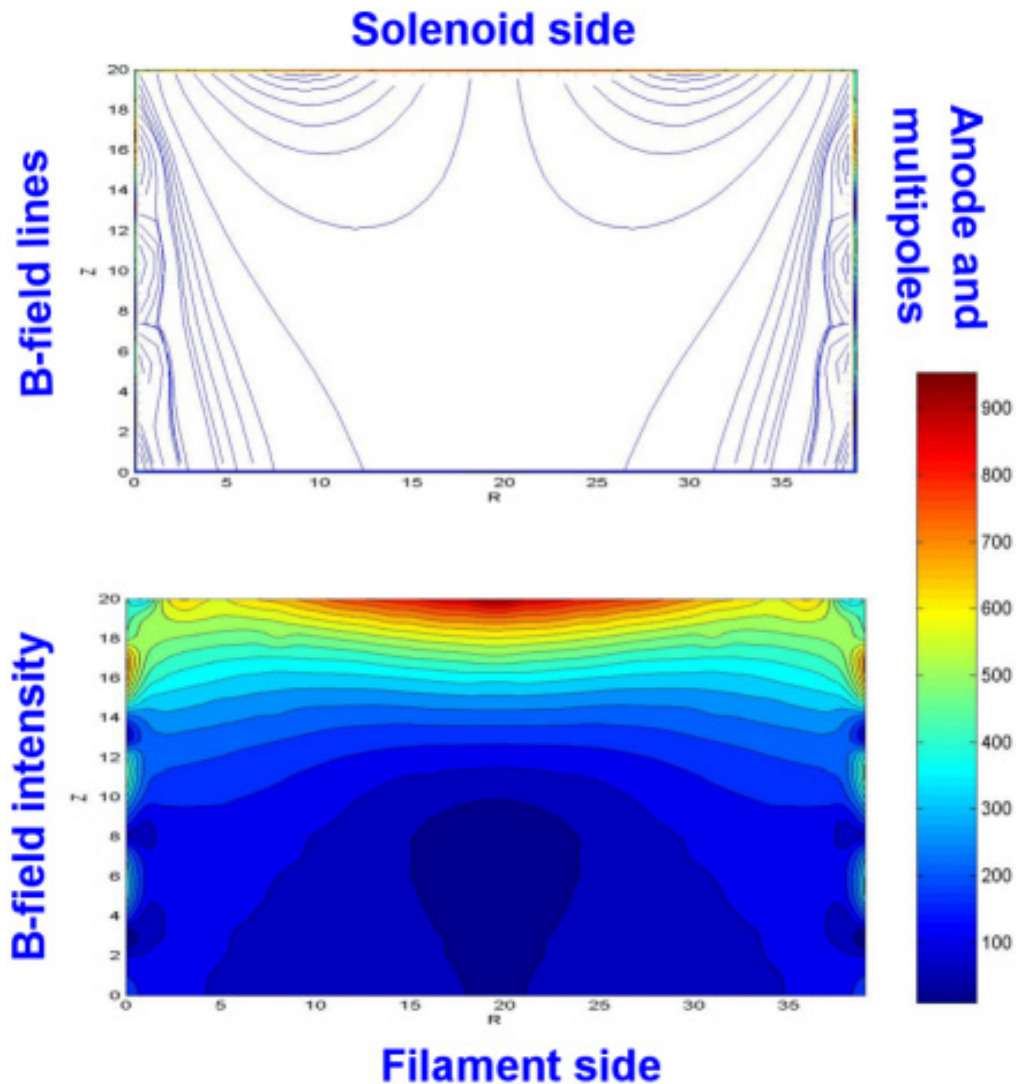
Figure 2. Map of the magnetic field lines in the central part of the main chamber on an horizontal plane passing through the longitudinal axis of the device. Here z is along the axis, while the colour scale unit is given in mV, which corresponds approximately to 2×10^{-5} T. This magnetic configuration prevents direct connection between the cathode and the linear part of the device.

The magnetic field strength B_s in the solenoid is another operating parameter of the device. The magnetized plasma column under study is produced by energetic electrons injected from the main chamber. A network of equally spaced permanent magnets is located on the anode, while two external coils allow shaping of the magnetic configuration in the main chamber. An experimental map of the magnetic field obtained through two perpendicular Hall sensors is displayed in figure 2. The map shows the magnetic field configuration on a horizontal plane of the main chamber at a height corresponding to the solenoid axis. Such a configuration prevents primary electrons from the cathode to directly enter into the linear part of the device. The reflexion of the primaries on the multipolar magnetic walls inside the source chamber allows a randomization of the trajectories

of the ionizing electrons and leads to a homogeneous flux at the entrance of the solenoid. As a result, a very stable, well-thermalized and homogeneous plasma column is obtained in this region.

Mean electron density is longitudinally and poloidally uniform, while radially peaks on the axis, reaching values in the range $n_e = 5 \times 10^8$–$2 \times 10^{10}\,\mathrm{cm}^{-3}$. The averaged electron temperature T_e is about 2–4 eV and ions stay cold ($T_i \leqslant 0.1\,\mathrm{eV}$). The injected negative space charge on the axis provides the source for a radial electric field, which makes the plasma column rotating at the $\mathbf{E} \times \mathbf{B}$ poloidal velocity [27].

In these experiments, aimed to study the structures in a cylindrical rotating plasma column, the plasma has been confined to the linear part of the solenoid (length $L = 1.2$ m) by a collecting circular electrode, with two segmented annular sections, each separately biased ($R_1 = 8$ cm, $R_2 = 16$ cm). In this situation, the plasma is not subjected to any curvature or $\nabla \mathbf{B}$ drift. In order to study the different diffusion or convection mechanisms across the magnetic field, the plasma column is restricted to 14 cm in diameter by a metallic diaphragm (limiter) just behind the grid at the entrance of the linear part. With this arrangement the experimental setup in the device is similar to some extent to the physical situation taking place in the tokamak SOLs. Indeed, behind a plasma limiter in toroidal fusion devices, the existence of strong radial electric fields induces a poloidal rotation and the formation of shear layers.

We have performed our measurements fixing the operating conditions ($V_b = 24$ V, $I_f = 96$ A, $B_s = 0.02$ T), even though the exact plasma parameters can be influenced by discharge parameters such as the cathode–anode bias, the filament current or the magnetic field strength of the solenoid and of the two compensating coils [27]. Other control parameters are the potential of the anode compared to the grounded chamber walls, those of the inner and outer region of the collecting plate and the grid bias. With the end plate globally grounded, we have observed that driving the anode potential negative leads to the onset of low frequency unstable waves, only when the grid was floating or negatively biased. We have previously reported on an $m = 2$ poloidal mode with a rotating spiral structure [27]. In the present experiments, the grid is kept floating, while the anode potential is kept negative ($V_a = -18$ V). The control parameter is then the potential of the inner part of the collecting plate, while the outer potential turns out to be not so critical ($V_{out} \sim 10$ V with respect to ground). Transition from the $m = 2$ mode, first goes through an $m = 1$ mode and then reaches a weak turbulence regime as the potential V_{in} is decreased from 30 to 25 and subsequently to 20 V. The peak electron density increases by 50% while the floating potential on the axis is only slightly decreased by about 1.5 V. Similar transitions have been reported in other devices closely resembling our setup [17]. Measurements reported below have been collected in the turbulent regime. Coordinate z is along the axis of the solenoid, while in the poloidal section r is horizontal (along the probe moving direction) and y is in the vertical direction.

3. Diagnostics

Averaged and fluctuating plasma parameters in the turbulent state have been measured by means of Langmuir probes. Shielded cylindrical probes with small tip (length 3 mm, diameter 0.5 mm) have been employed. Scanning of almost the whole poloidal cross-section (diameter 30 cm) could be performed through an L-shaped probe moving radially and rotating about its axis, located at a longitudinal position $z = 100$ cm from the grid (see figure 1). Probe positioning in

the poloidal section is achieved by an automated system of two stepper motors. A second probe, movable only along the radial direction is used as a reference and has been inserted at different longitudinal positions ($z = 30, 50, 80$ cm). Two kinds of measurement have been performed. In the first case, time series of the electron saturation current of the reference as well as of the scanning probe have been recorded at the same time on a digital scope. The sampling time was varied from 1 to 4 μs. The record length has been 5×10^4 points. Mean data have been obtained by averaging over the whole time series. The electron saturation current was measured as a voltage drop on a shunt resistance (~ 2 kΩ) with a probe bias held constant at +18 V by batteries, in order to be well above the mean plasma potential measured in the whole section of the device. Verification of the results, both by changing the probe biasing to +9 V and detecting the ion saturation current have been performed too, to ensure that the measurements can be ascribed effectively to plasma density fluctuations. Time series of the floating potential of the probes have been measured too. However, in the region outside the plasma column, we observe that the shape of the pulses depends strongly on the impedance of the probe circuitry (normally the 1 MΩ input impedance of the digital scope). Problems arising in the measurement of the floating potential in presence of moderately high-frequency fluctuations have been anticipated in [31]. In particular, we detect long decay times (i.e. longer than the width of pulses observed in the electron saturation current time series) after a strong pulse arrives at the probe. This obviously prevents a direct measurement of the electric field inside the plasma structures by taking the difference of two nearby floating potential measurements. This also prevents us from having direct information on local $\mathbf{E} \times \mathbf{B}$ drifts. Such a drawback could be quite general and we suggest that information based on floating potential analysis could be often biased due to insufficiently high impedance and low capacitance of the probe as our measurements pointed out. A suitable spectroscopic diagnostic for detecting ion rotation velocity in Mistral is currently under development and could be operated in the near future. However, in this first stage, we have implemented another set of measurements aimed at gaining information about the local plasma potential, by recording the full Langmuir characteristics of the probes and resampling it inside the detected events. Recording of the averaged characteristics has been performed too, by slowly sweeping the probe potential (40 V swept in 10 s). Data have been analysed in order to extract directly the mean electron temperature (from the slope of the exponentially rising part of the characteristic) and the mean plasma potential (from the inflection point in the characteristic).

In order to study the spatio-temporal evolution of the structures, a conditional sampling analysis has been implemented [32]. The analysis is performed online on the electron saturation current data, requiring that a particular condition is met in the reference probe time series (such an event triggers the selection of a fixed time window out of the scanning probe time series [32]). A hundred time windows of the electron saturation current, about 500 μs long, have been acquired and averaged for each position in the poloidal cross-section, yielding to the reconstruction of the time evolution in the whole plasma section (from a grid of 225 positions, with a resolution of 1.5 cm in a typical case). Contrary to standard practice, in which events are selected requiring simply that the signal crosses a fixed level (normally of a few standard deviations from its mean value [7, 32]), we found it necessary to impose a more stringent condition on the shape of the whole pulse selected. A range of amplitude and shape (rising and falling time) is selected. This produces a very efficient pattern selection inside the turbulence using a structure template. This leads to a sharper definition of the structures and to a reduced smearing, drawbacks inherently affecting conditional sampling analysis. The improvement achieved in averaging only structures with a well-defined pattern can be assessed in figure 3. In the upper part of figure 3, indeed, one
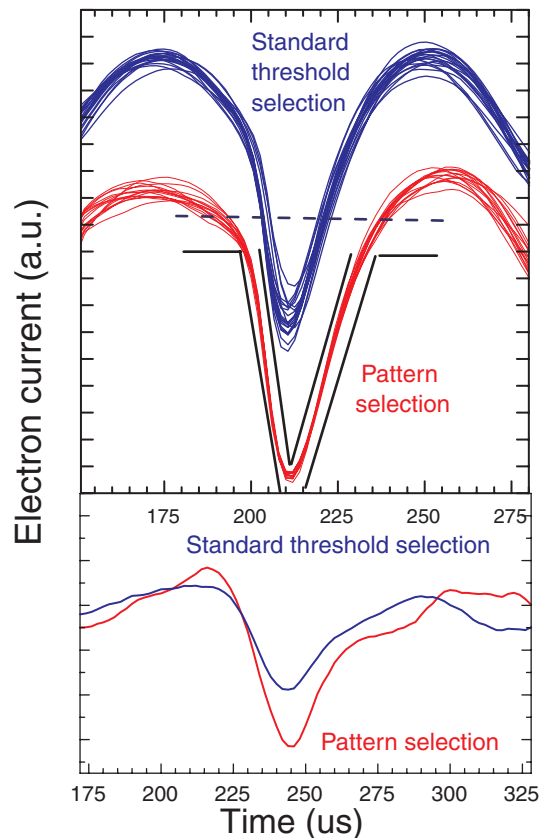
Figure 3. Above: the averaged time windows selected in the reference probe time series during the scan of the 225 grid positions in the poloidal section. The envelope in the case of a pattern selection trigger is clearly sharper compared to the one obtained with a standard threshold trigger. Below: the conditionally sampled time window recorded at one position in the column edge (red, pattern trigger; blue, standard threshold one) shows the improvements that can be achieved.

can compare the averaged time windows recorded during the scan of the 225 grid positions when a threshold or a selected pattern trigger is employed. The improvement in one of the conditionally sampled time window can be assessed from the lower part of figure 3: not only is the signal to noise ratio improved, but also features like the shoulder in the pulse decay can be detected. Moreover the overall stability of the reference signal during the scan can be guaranteed by using such an enhanced conditional sampling recipe. Further developments of this technique are planned in order to extract important statistical information about the turbulent state. Changing several parameters in defining the shape of the pattern would give new informations on the structure of the turbulence. The detection of fully turbulent states could be obtained in a more precise way compared to the classical calculation of skewness, flatness and higher moments analysis.

We tried also to measure directly the electric field inside the structures. For this purpose, we have acquired conditionally sampled time window of the full Langmuir characteristics by performing repeated conditional sampling averages (20) during the slow sweep of the probe potential (30 V with a step of 0.5 V). Since the whole procedure is now quite slow, we have sampled only a limited area of the poloidal section ($5 \times 5\,cm^2$) in order to avoid discharge stability problems.
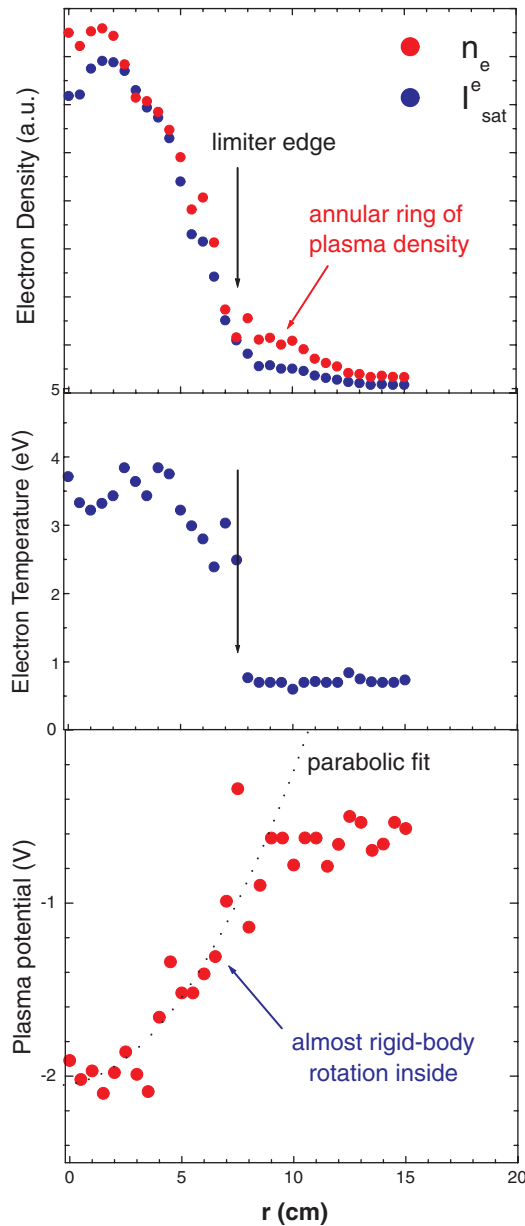
Figure 4. Mean electron saturation current, density, temperature and plasma potential radial profiles measured in the weak turbulence regime. The appearance of a circular corona of plasma around the plasma column is displayed.

4. Discussion of the experimental results

Mean radial profiles have been obtained by averaging the recorded time series, both for the electron saturation current and for the floating potential. We recorded also averaged full Langmuir characteristics. Profile of the electron density, temperature and plasma potential have been extracted and are shown in figure 4.

Electron temperature decreases abruptly to almost zero at the limiter (the minimum sensitivity being 0.33 eV due to the finite size of the steps in the probe potential sweeping). Mean electron density profiles substantially agree with that of the electron saturation current. The main feature of the density profile is the presence of an annular plateau surrounding the plasma column. Since electron temperature is less than 1 eV in the limiter shadow, no ionization can occur and plasma will be continuously transported there due to diffusive or convective flows from the central column. It is also worth to notice that the density gradient peaks in correspondence of the limiter position. This situation is indeed very similar to the edge and pedestal region in the magnetic-fusion devices. Plasma column displays a radial potential, well centred on the solenoid axis. Mean potential profiles are approximately parabolic inside the limiter leading to an almost rigid body $\mathbf{E} \times \mathbf{B}$ rotation of the plasma column. On the other hand, the potential profile flattens behind the limiter and the $\mathbf{E} \times \mathbf{B}$ velocity drops. This leads to the formation of the velocity shear layer behind the limiter. The build-up of this radial electric field is a consequence of the non-ambipolar transport induced by the end-plates' biases. This is probably connected to the polarization drift [33], which is restricted to a thin layer (of the order of the ion Larmor radius) outside the column. Since only the fast electrons are lost axially inside this layer, this also explains the recorded rapid radial decrease of the electron temperature.

An inspection of the electron saturation current time series recorded in the region outside the limiter shows the onset of intermittent pulses very large with respect to the mean values there. On the other hand, in the internal region, fluctuations appear to be smaller and with a more regular oscillating and quasi-periodic pattern. We have recorded simultaneously the time series of both the scanning probe and the reference probe when they were held at the same position in the poloidal section. This was repeated for all the three longitudinal positions available for the reference probe. In each case, the comparison of the time series shows that no temporal delay can be detected. Also the pattern of the signals appears to be the same. Since the longitudinal distance of the two probes is comparable with the length of the plasma column, this is suggesting that we are observing an almost flute-like structure.

As for the conditional sampling analysis of the electron saturation current time series, the reference probe is placed in correspondence to the limiter position, i.e. at $r = -6$ cm and $y = 2$ cm in the poloidal section coordinate. This choice of the reference probe location allows us to trigger the rise of the structures propagating in the edge. The results of the conditional sampling analysis, with the triggering condition already described in the previous section, is shown in figure 5 for a discharge operated at a pressure of 9×10^{-3} Pa. Time step was 2 μs and space resolution was 1.5 cm. A movie with the complete data set is available.

The rotation of the plasma column (with approximately a 200 μs period) can be appreciated from the slightly eccentric motion (radius 1 cm), evidenced also by the movement of the electron saturation current baricentre shown in figure 6. This has been estimated by the average position of the grid points weighted with the measured values of the electron saturation current

$$\langle \vec{x} \rangle = \frac{\sum_i (I_{sat}^e)_i \vec{x}_i}{\sum_i (I_{sat}^e)_i}.$$

This approximately corresponds to the centre of the electron pressure distribution on the plasma column cross-section.

However the most striking feature is the expulsion of a bent tail of plasma, which we called a plasma burst, from the central column. The burst evolves along a spiral trajectory around the column, as can be seen from figure 6. There the time evolution of the mean position of the plasma
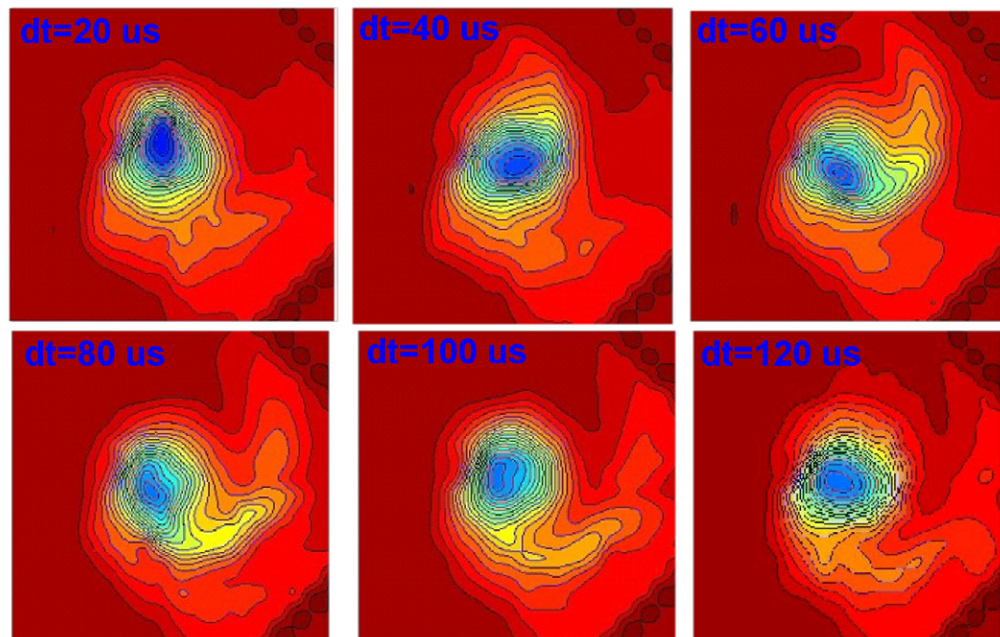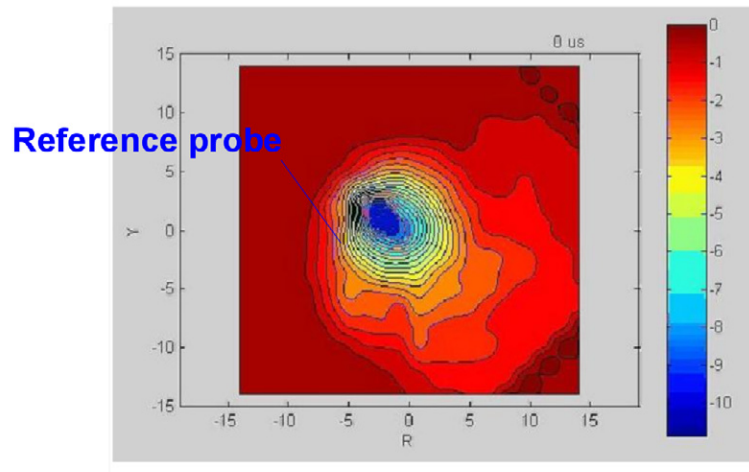
Institute *of* **Physics** Φ DEUTSCHE PHYSIKALISCHE GESELLSCHAFT

Figure 5. Electron saturation current contour plot obtained by enhanced conditional sampling. Each frame is delayed by $10\,\mu$s, lines correspond to values 1.5, 2, 2.5, 3, 4, 5, 7, 9 for display purposes. The development of a spiral tail with the radial convection of plasma to walls and its subsequent decay during the column rotation is shown.

in the edge region can be observed. This is evaluated by averaging only the position (using the polar coordinates) of the grid points in the edge region, weighted with the measured values of the electron saturation current. This approximately corresponds to the centre of the electron pressure structure developing in the plasma column edge. The bending of the radially moving burst in a spiral arm is due to the rotation velocity decrease along the radius. The winding up of the tail ends when the structure reaches the walls and the plasma gets lost, after about $130\,\mu$s.
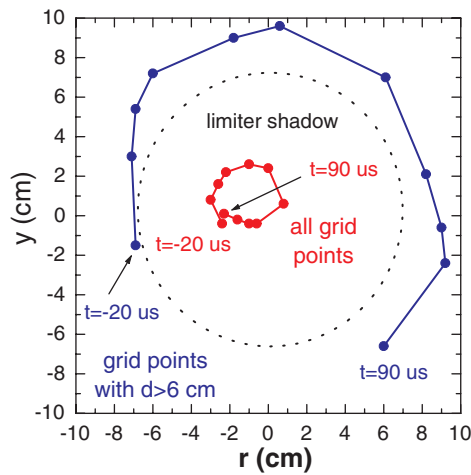
Figure 6. Time evolution of the position of the electron saturation current weighted average for the whole plasma column (red) and for the edge structure (blue). The latter is estimated by weighting only the electron saturation current values recorded at grid points located in the column edge, that is the region $d = \sqrt{r^2 + y^2}$ ($\geqslant 6\,\text{cm}$).

We have taken several different conditionally sampled dataset in the same discharge conditions by changing the size or the shape of the triggering pulses in the reference probe time series. Even if this influences the velocity of the recording procedure, then it should produce the same kind of spatio-temporal behaviour. Even by using a traditional two standard deviation triggering condition for the reference probe, we have obtained a similar pattern of evolution, albeit the picture appears more confused and noisy probably due to higher smearing effects using the standard technique.

As already stated, in the region of the poloidal section inside the limiter, the electron saturation current fluctuations are not much skewed and almost symmetric, with both positive and negative pulses. In principle each of these signatures could correspond to a different kind of structure. In order to check this point, we have selected events in the same discharge conditions triggering first on positive pulses and then on negative ones. However the conditionally averaged time series appear to be the same in both cases apart from a fixed time delay. Such a delay corresponds almost exactly to a quarter of the period of the plasma column rotation. This can be understood if the oscillations in the reference probe time series in the region inside the limiter are mainly due to the eccentric rotation of the central plasma column.

Another interesting observation is related to the effect of the neutral argon pressure. Indeed, even if at a pressure $P = 1.2 \times 10^{-2}$ Pa the event looks very similar to the one pictured in figure 5, at $P = 1.5 \times 10^{-2}$ Pa the eccentricity of the baricentre rotation becomes smaller (with radius ~ 0.5 cm). Moreover at pressures $P = 1.8 \times 10^{-2}$ Pa and 2.2×10^{-2} Pa, the eccentric rotation almost disappears and no tail formation could be detected.

We have also recorded in the same discharge conditions conditionally sampled events with different radial locations of the reference probe, that is at $r = -14, -10, -6, -4, -1$ cm. The detected events look similar in all the cases, even if the time series out of which the pattern
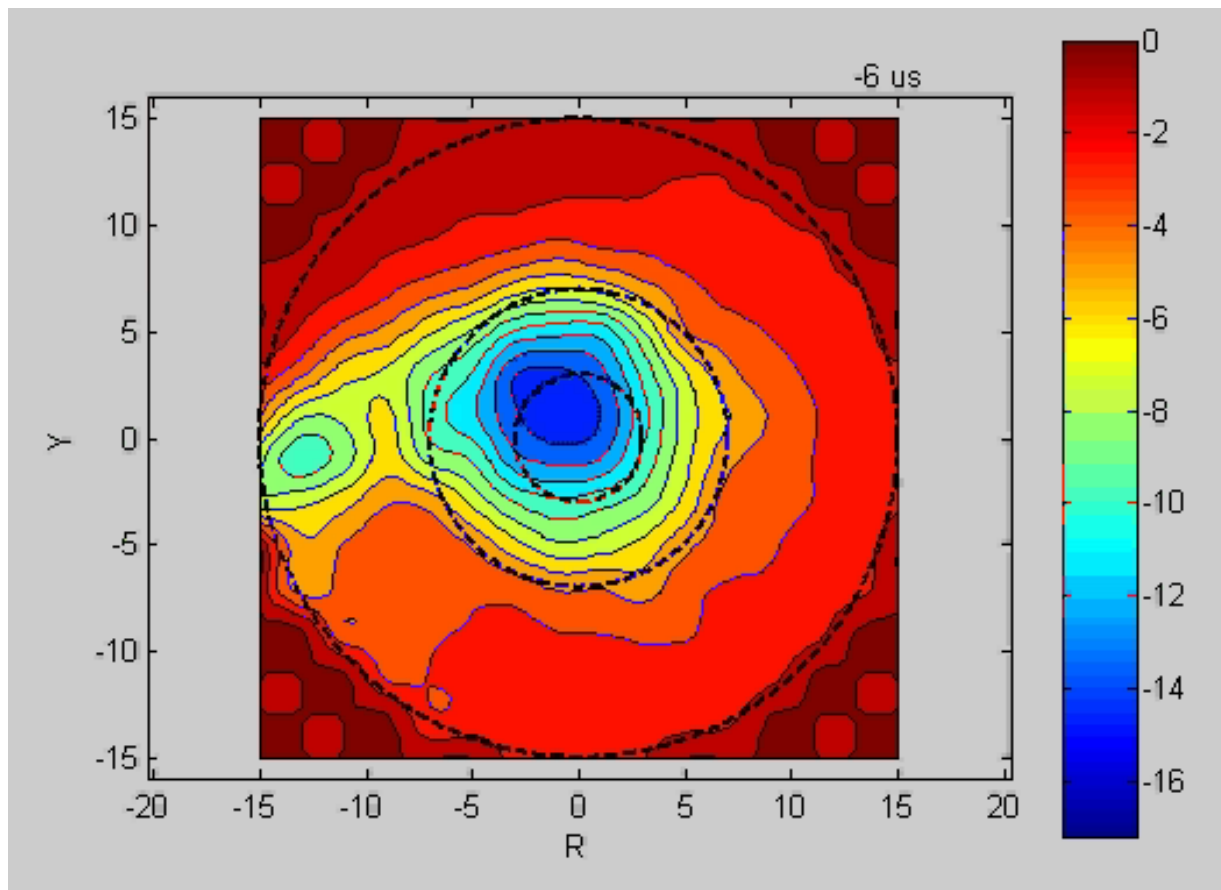
Figure 7. Electron saturation current contour plot obtained by enhanced conditional sampling with the reference probe located well behind the limiter ($r = -14$, $y = 0$). The picture refers to a time close to when the structure passes also by the reference probe. A well-developed bent arm, looking similar to the one shown in figure 5, is displayed.

selection is performed differs significantly in their statistical properties [34]. Only the event triggered at the centre of the column fails to show a spiral tail development, thus suggesting a lack of correlation with the edge of the column where the perturbation develops. A more evident detachment of the plasma density burst from the column can be observed in the events triggered in the region well outside the limiter. This can be grasped in the picture shown in figure 7 as well as in the movie. However this apparent detachment could be due also to an artefact caused by the smearing arising from a lack of sufficient spatial coherence or to a jittering in the tail developing times, since now triggering happens at a delayed time with respect to the time when perturbation starts growing.

Density burst features with spatial scales of a few millimetres have been reported in the literature [6]. This is not the case in our experiments. An event recorded with a higher spatial resolution of 0.5 cm (close to the limit set by the probe tip dimension), in the region outside the limiter, shows that the tail is a smooth structure with a bell shape in the transverse direction, as
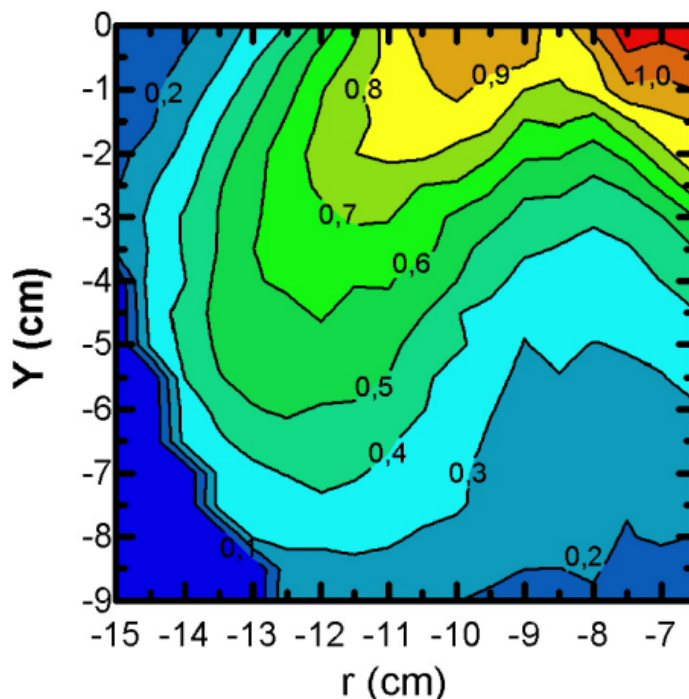
Figure 8. High-resolution contour plot of the tail structure obtained by enhanced conditional sampling.

it appears from figure 8. Again a movie with the spatio-temporal evolution of the tail structure is available.

In order to study the plasma motion inside the structure, we need information about the local electric field. Experimentally, this is often achieved through the recording of the floating potential time series. This in turn neglects electron temperature fluctuations, which could not be always justified. Moreover, as already stated, in Mistral we observe long tails in the electric signal of a floating probe after a density pulse. This prevents us to use these signals for the measurements of the local electric field. We have addressed such a problem performing a conditional sampling of the full Langmuir characteristics of the probe, as discussed in the previous section. The measurements have been limited to a small area of $5 \times 5\,\text{cm}^2$ of the poloidal section just across the limiter, with a resolution of 0.5 cm.

The spatio-temporal evolution of the electron density structure is similar to that already observed in the electron saturation current time series. The results for the electron density, temperature and plasma potential are shown in figure 9 at three times during the passage of the plasma density burst. In the central picture, a density blob, which will gives rise to the spiral arm structure, shows up, while the plasma column moves upwards in its eccentric rotation frame. As seen from the results on the electron temperature in the left panels, the structure is also convecting energy in the edge of the plasma column. In the right panels, it is possible to appreciate the perturbation of the plasma potential map induced by the column motion and by the formation of the blob. The spatio-temporal evolution can be guessed from the map as one realizes that the $\mathbf{E} \times \mathbf{B}$ drift happens upwards along the potential field lines. In particular, plasma potential maps show that electrostatic potential rises as the structure arrives and decreases afterwards.
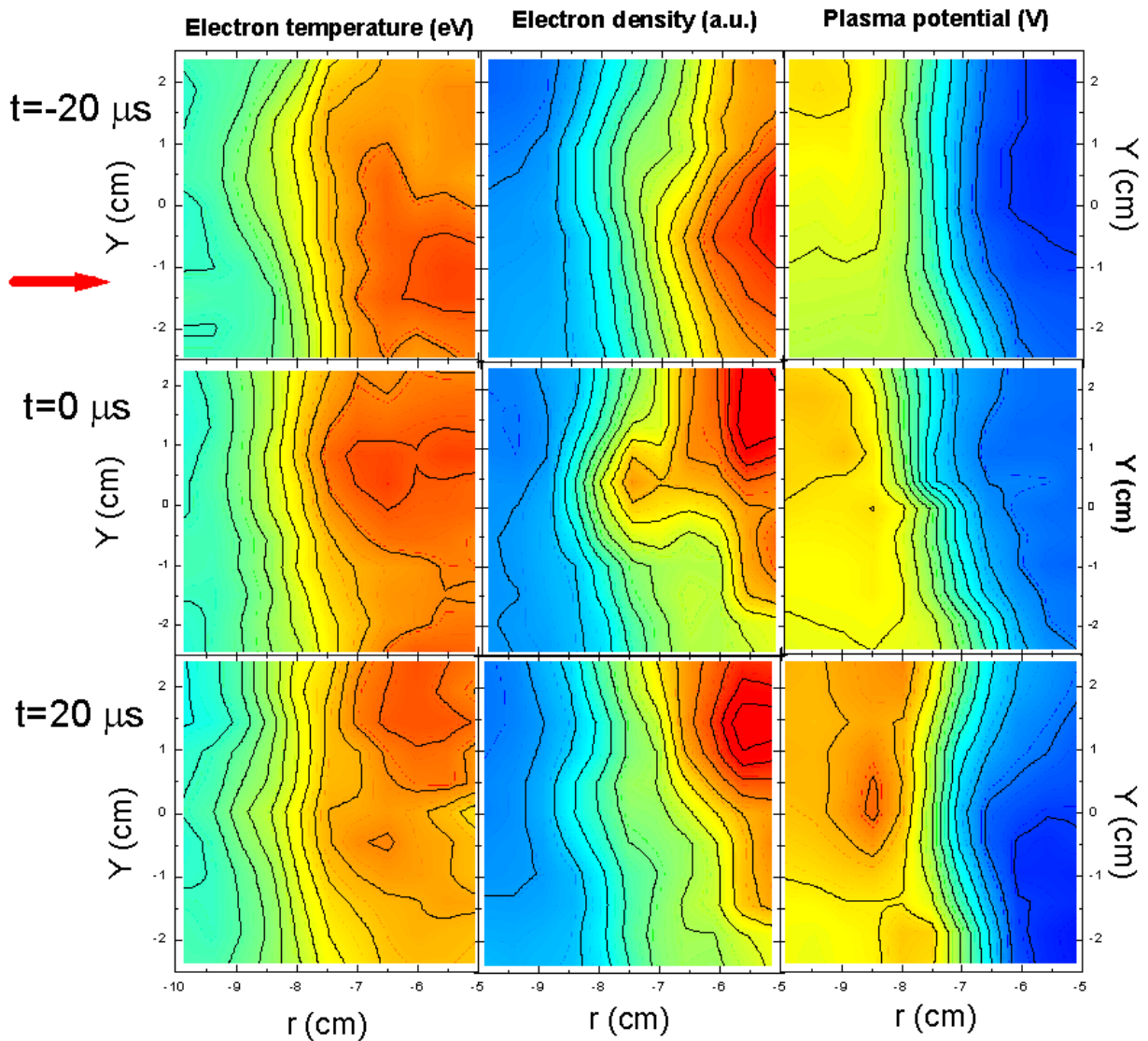
Figure 9. Electron density, temperature and plasma potential contour plot at three times during the passage of the structure. A linear colour scale from blue to red is employed: 0–5 eV for T_e, 0–200 for n_e and −10 to 0 V for V_p.

This can be appreciated more clearly by comparing the time series of electron density and plasma potential at a fixed position as in figure 10. Since the plasma column is rotating, the time series can be thought broadly as a map in the poloidal angle $\theta \sim \omega t$. Given this, one should realize that a poloidal electric field appears inside the structure, driving the radial convection of plasma outside the limiter and leading to the build-up of the spiral structure. Using the full bidimensional maps of the plasma potential, the poloidal and radial components of the instantaneous electric field have been extracted. The corresponding $\mathbf{E} \times \mathbf{B}$ drift velocity has been calculated and it is displayed in figure 11 at the time when the structure is passing by the horizontal axis (corresponding to the central frame in figure 9). Again a velocity component corresponding to plasma convection outside the limiter can be appreciated.
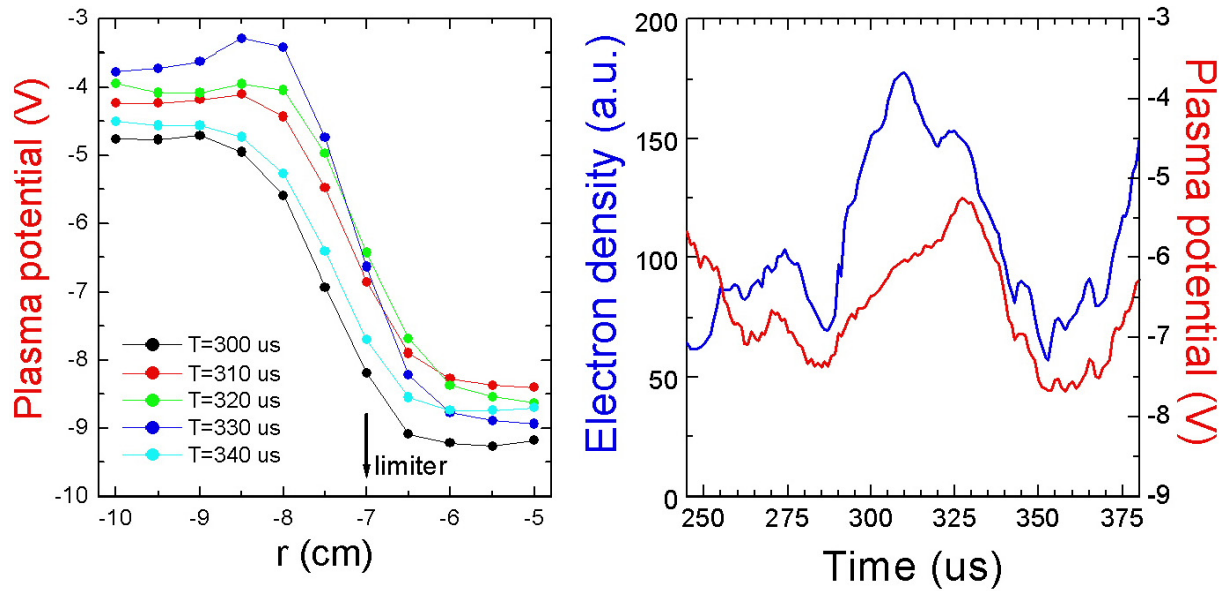
Figure 10. Left: modification of the plasma potential radial profile measured along the line $y = 0$ of figure 9. Right: conditionally sampled time series of electron density (blue) and plasma potential (red) measured at $r = -6.5$ cm, near the limiter position.
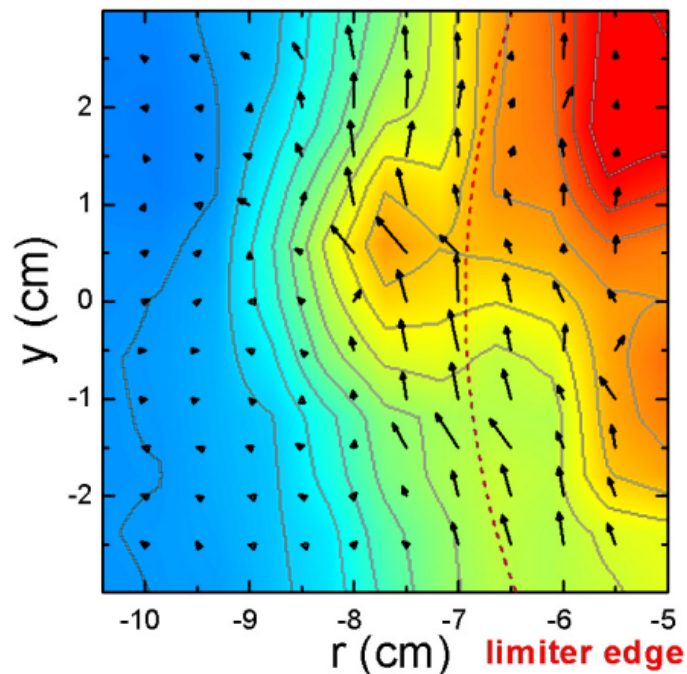

Figure 11. Contour plot of the $\mathbf{E} \times \mathbf{B}$ drift velocity extracted from the plasma potential map measured at the time the density structure, the superimposed contour plot, was passing through the horizontal axis. The linear colour scale from blue to red is the same as employed in figure 9 for the electron density.

5. Conclusions

We have performed a detailed analysis of the structures present in the turbulent regime of the device Mistral. Enhanced conditional sampling analysis shows the development of a density spiral tail emanating from the plasma column and extending outside the limiter towards the walls. This observation strongly suggests that plasma is radially convected inside such spiral structures. A conditional sampling analysis of the full Langmuir characteristics yielded the simultaneous reconstruction of both the electron density and the plasma potential time series. In this way the radial convection of plasma has been experimentally proved, showing the presence of a poloidal electric field inducing an $\mathbf{E} \times \mathbf{B}$ radial motion inside the structure [25].

From the theoretical point of view, our results, namely the development of an annular bursty plasma around the plasma column and the radial convection of plasma bursts, are in broad agreement with the expectations based on centrifugal effect simulations [23]. From a more general point of view, when fast rotating plasma layers develops, as in tokamak SOL regions, this effect can constitute a viable mechanism providing the necessary drive for the burst transport phenomena which is recently so much debated [4]. However, more experimental and theoretical insight is needed to reach a complete understanding of the matter.

Acknowledgments

References

[1] Antar G Y 2003 *Phys. Rev. Lett.* **91** 055002
[2] Boedo J A *et al* 2001 *Phys. Plasmas* **8** 4628
[3] Zweben S J *et al* 2002 *Phys. Plasmas* **9** 1981
[4] Antar G Y, Counsell G, Yu Y, LaBombard B and Devynck P 2003 *Phys. Plasmas* **10** 419
[5] Grulke O, Klinger T, Endler M, Piel A and W7-AS Team 2001 *Phys. Plasmas* **8** 5171
[6] Bleuel J, Endler M, Niedermeyer H, Schubert M, Thomsen H and W7-AS Team 2002 *New J. Phys.* **4** 38
[7] Oynes F J, Olsen O M, Pécseli H L, Fredriksen A and Rypdal K 1998 *Phys. Rev.* E **57** 2242
[8] Riccardi C and Fredriksen A 2001 *Phys. Plasmas* **8** 199
[9] Fredriksen A, Riccardi C, Cartegna L and Pécseli H L 2003 *Plasma Phys. Control. Fusion* **45** 721
[10] Greiner F, Block D and Piel A 2004 *Contrib. Plasma Phys.* **44** 335
[11] Nielsen A H, Pécseli H L and Rasmussen J J 1996 *Phys. Plasmas* **3** 1530
[12] Antar G Y, Krasheninnikov S I, Devynck P, Doerner R P, Hollmann E M, Boedo J A, Luckhardt S C and Conn R W 2001 *Phys. Rev. Lett.* **87** 065001
[13] Spolaore M, Antoni V, Cavazzana R, Regnoli G, Serianni G, Spada E and Vianello N 2002 *Phys. Plasmas* **9** 4110
[14] Martines E, Hron M and Stockel J 2002 *Plasma Phys. Control. Fusion* **44** 351
[15] Carbone V, Regnoli G, Martines E and Antoni V 2000 *Phys. Plasmas* **7** 445
[16] Boedo J A *et al* 2003 *Phys. Plasmas* **10** 1670
[17] Klinger T, Latten A, Piel A, Bonhomme G, Pierre Th and Dudok de Wit T 1997 *Phys. Rev. Lett.* **79** 3913

Institute *of* **Physics** ⬮ DEUTSCHE PHYSIKALISCHE GESELLSCHAFT

[18] Grulke O, Klinger T and Piel A 1999 *Phys. Plasmas* **6** 788
[19] Lehnert B 1964 *Dynamics of Charged Particles* (Amsterdam: North-Holland)
[20] Horton W and Liu J 1981 *Phys. Fluids* **24** 1270
[21] Ekdahl C, Bartsch R R, Commissio R J, Gribble R F, McKenna K F, Miller G and Simon R E 1980 *Phys. Fluids* **23** 1832
[22] Krasheninnikov S I 2001 *Phys. Lett.* A **283** 368
[23] Paulsen J V and Benkadda S 2002 *Proc. 9th EU-US TTF Workshop* (*Cordoba*) (http://www-fusion.ciemat.es/ttf2002)
[24] Ellis R F, Hassam A B, Messer S and Osborn B R 2001 *Phys. Plasmas* **8** 2057
[25] D'Ippolito D A, Myra J R and Krasheninnikov S I 2002 *Phys. Plasmas* **9** 222
[26] Krasheninnikov S I, Smolyakov A I and Soboleva T K 2005 *Czech. J. Phys.* **55** 307
[27] Matsukuma M, Pierre Th, Escarguel A, Guyomarc'h D, Leclert G, Brochard F, Gravier E and Kawai Y 2003 *Phys. Lett.* A **314** 163
[28] Kono M and Tanaka M Y 2000 *Phys. Rev. Lett.* **84** 4369
[29] Pierre Th, Escarguel A, Guyomarc'h D, Barni R and Riccardi C 2004 *Phys. Rev. Lett.* **92** 065004
[30] Brault C, Escarguel A, Koubiti M, Stamm R, Pierre Th, Quotb K and Guyomarc'h D 2004 *Proc. 12th Int. Congress on Plasmas Physics* (*Nice*) (http://hal.ccsd.cnrs.fr)
[31] Light M, Chen F F and Colestock P L 2001 *Phys. Plasmas* **8** 4675
[32] Pécseli H L and Trulsen J 1989 *Phys. Fluids* B **1** 1616
[33] Naulin V 2002 *New J. Phys.* **4** 28
[34] Magni S, Roman H E, Barni R, Riccardi C, Pierre T and Guyomarc'h D 2005 *Phys. Rev.* E **72** 026403